Overhead Transmission Line Sag Monitoring Using a Chirped-Pulse Phase-Sensitive OTDR

Jorge Canudo, Pascual Sevillano, Andrea Iranzo, Sacha Kwik, Javier Preciado-Garbayo, and Jesús Subías

***Abstract*—The capacity of overhead transmission lines is fixed and determined by the physical properties of the line, which are estimated based on worst-case weather scenarios. Exceeding the capacity limit can cause the conductor to increase the sag excessively, bringing it too close to the ground and creating a safety risk. Real-time monitoring of the sag value enables dynamic capacity configuration, thereby reducing safety risks and improving the efficiency of the transmission line. Distributed acoustic sensing based on chirped-pulse phase-sensitive optical time-domain reflectometry (CP-ΦOTDR) can be used to measure the vibration induced by wind on the cable line taking advantage of the optical fiber already deployed in the power line. An analysis of the recovered strain in the frequency domain reveals multiple frequency components related to the cable's current mechanical state. By identifying the fundamental frequency, it becomes possible to quantitatively calculate the sag. Tracking the central frequency of each span allows for the monitoring of the sag for each span of the line using just one single-end interrogator.**

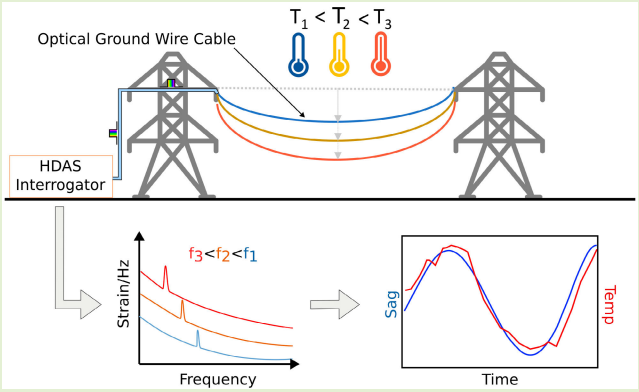

***Index Terms*—Distributed acoustic sensing, overhead line monitoring, phase-sensitive optical time-domain reflectometry (OTDR), Rayleigh scattering, sag measurement.**

I. Introduction

With the growing demand and the increase of diverse energy sources, traditional electrical networks have suffered a transformation toward smart grid systems. Renewable energy sources have created a decentralized energy landscape that demands smart management of supply fluctuation. Optimization of line capacity is one of the most critical tasks in this framework. The current transmission capacity depends directly on sag [1], which is one of the most limiting parameters in the system's configuration. Sag is defined as the vertical distance between the midpoint of the strained conductor and the direct line between the insulators placed in its two suspension points [2]. This sag is deliberately introduced to reduce tensions suffered in the overhead conductor's rest points, which can lead to tower damage if excessive [3], [4]. Sag implementation in overhead power lines demands rigorous control of its value as an excessive increase of sag may result in the line being too close to the floor, allowing for ground discharges to happen if some object with relevant height passed below the overhead line [5]. Due to heat derived from current conduction, environment temperature variations, heat interchange with wind, and other extreme phenomena, sag is a variable parameter. Overhead power lines are designed with high-security coefficients based on the worst-case scenario of weather conditions [6]. However, these worst-case scenarios may not occur frequently, and so the line may be underutilized for much of the time. A precise sag monitoring can lead to a dynamic adjustment of the capacity limit of the line, based on its actual operating conditions and without compromising security [7].

Actual sag estimation techniques are based on the correlation of this parameter with physical properties, which

Manuscript received 21 July 2023; revised 23 October 2023; accepted 27 November 2023. Date of publication 13 December 2023; date of current version 12 January 2024. This work was supported in part by Red Eléctrica de España Sociedad Anónima Unipersonal (SAU) and Aragón Photonics Labs Sociedad Limitada Unipersonal (SLU) under Project MISTRAL, in part by the Spanish MCIN/AEI/10.13039/501100011033 and Fondo Europeo de Desarrollo Regional (FEDER) under Grant DI-17-09169, and in part by the Government of Aragón (Reference Group T20_23R). The associate editor coordinating the review of this article and approving it for publication was Prof. M. Jaleel Akhtar. *(Corresponding author: Jorge Canudo.)*

Jorge Canudo, Pascual Sevillano, and Jesús Subías are with the Department of Applied Physics, Universidad de Zaragoza, 50009 Zaragoza, Spain (e-mail: jcanudo@unizar.es; psevi@unizar.es; jesus.subias@unizar.es).

Andrea Iranzo and Javier Preciado-Garbayo are with Aragon Photonics Labs SLU, 50009 Zaragoza, Spain (e-mail: a.iranzo@aragonphotonics.com; j.preciado@aragonphotonics.com).

Sacha Kwik is with Red Eléctrica de España SAU, 28109 Alcobendas, Spain (e-mail: sacha.kwik@ree.es).

Digital Object Identifier 10.1109/JSEN.2023.3340296

can be measured directly with different single-point sensors. For instance, sag can be related to temperature; therefore, by knowing the thermal properties of the conductor materials, it is possible to estimate its sag according to [8]. Tension of the power conductor is another method to obtain a value for this parameter [9]. Direct observation via cameras and GPS [10], [11], laser [12], or the use of an inspection robot [13], [14] are other solutions to the sag measurement problem. Vibrations in the overhead power line contain information on how long the cable is, which directly leads to its sag value [15], [16]. Since most of the power lines are suspended and continuously exposed, they can be subjected to various types of vibrations induced by wind. These can range from generic eolian vibrations to specific phenomena such as galloping [17]. Eolian vibrations result from transverse and laminar wind flow around the cable, creating vortexes that alternate between the upper and the lower parts of the conductor. The frequency of these vibrations is fixed and depends on wind velocity and the conductors' diameter [18]. Vortexes created by eolian vibrations can excite one of the harmonic vibrational modes of the cable in the span, which are determined by its physical and mechanical characteristics such as weight and length [19], [20]. Notably, lower vibration frequencies in overhead power lines correspond to greater sag [21]. Some of the aforementioned sensors rely on electronic transducers that can be affected by electromagnetic interference. To address this problem, optical sensors based on fiber Bragg gratings (FBGs) have been proposed [22], [23]. This technology allows for both temperature [24], [25] and tension [26], [27] measurements, which are the main parameters involved in sag evolution in overhead power lines. The use of this optical sensing technology overcomes the electromagnetic interference challenge, but as with all the aforementioned sag estimation methods, it requires at least one measurement device per monitored span. This requirement increases the complexity of a smart sag monitoring system due to the coordination between the individual sensors, and the investment in the deployment and maintenance of each one of them.

To address this problem, a distributed measurement is proposed in this work, which reduces the number of required devices to approximately one every 40 km [28], and takes advantage of the optical fiber already deployed within the cables. To achieve this, a distributed acoustic sensor (DAS) is used to measure strain throughout the optical fiber, registering its variations over time. This temporal information is then transformed into the frequency domain, allowing information on the cable vibrations induced by the wind to be retrieved. According to [29], these vibrations can vary based on wind velocity and the conductor's diameter, but there are also other vibrational modes that tend to resonate with the fundamental frequency and harmonics of the span, resulting in certain low frequencies with greater vibrational amplitudes. Since these frequencies are primarily determined by the length of the conductor, they are closely related to its sag. By detecting and tracking changes in these frequencies over time, it is possible to develop a technique for monitoring the sag of the conductor.

II. Measurement Principle

Optical time-domain reflectometry (OTDR) offers several advantages for large infrastructure monitoring over electronic alternatives. They enable distributed sensing over long distances at a reduced cost as the optical fiber acts as both a sensor and an information carrier. This reduces the number of measurement devices required and also provides immunity to electromagnetic interference [30], [31], [32], [33]. When a highly coherent pulsed laser is used as a light source, the interference of the Rayleigh backscattered light from the scattering centers covered by the optical pulse generates a jagged profile. Minute perturbations in the fiber can generate local changes in the refractive index that yield random amplitude variations in the registered signal [34], [35], [36]. This technique, commonly referred to as phase-sensitive OTDR (ΦOTDR), detects and locates external perturbations close to the fiber by analyzing the variation of backscattered intensity trace between pulses. Although the technique exhibits high sensitivity, there is a nonlinear relationship between the amplitude of the perturbation and the variation in the retrieved signals [37]. Demodulating the phase from the ΦOTDR signal using I/Q demodulation and homodyne detection could lead to a quantitative measurement of the perturbation amplitude [38]. However, the system performance in this architecture is still limited by the 2π periodicity of the phase and the presence of fading points. Chirped pulse ΦOTDR (CP-ΦOTDR) technology can linearly retrieve the amplitude of the external perturbation solving both of the mentioned problems present in conventional ΦOTDR.

By performing a linear variation of the emission frequency of the source within the pulse, the CP-ΦOTDR system can resolve strain-induced variations in the refractive index. The technique is based on the estimation of local temporal delay Δt present in the trace generated by perturbation-induced spectral shift $\Delta\nu$ [39]. This Δt can be related to ongoing strain perturbations through its relationship with the refractive index [40]. As the measurement principle is not directly related to the intensity of the backscattered trace, the signal-to-noise ratio (SNR) on the CP-ΦOTDR does not exponentially decay with sensing distance as it does in conventional ΦOTDR. Equation (1) shows how strain variations, $\Delta\varepsilon$ [ε], are obtained from local temporal shifts in the trace, Δt [s] [39], [41]

$$-\left(\frac{1}{\nu_0}\right)\left(\frac{\delta\nu}{\tau_p}\right)\Delta t = \frac{\Delta\nu}{\nu_0} \approx -0.78\Delta\varepsilon \tag{1}$$

where ν_0 [Hz] stands for the central frequency of the pulse, τ_p [s] stands for the temporal width of the pulse, $\delta\nu$ [Hz] stands for the spectral content of the linearly chirped pulse, and $\Delta\nu$ [Hz] stands for the laser frequency change that compensates the strain variation [40].

III. Data and Measurements

Measurements were conducted on the María-Fuendetodos overhead line (Fig. 1), located in northeast Spain and operated by Red Eléctrica de España. The line, 31.8 km long with 85 spans, facilitates the evacuation of energy generated by a nearby wind turbine installation. It has two double-circuit

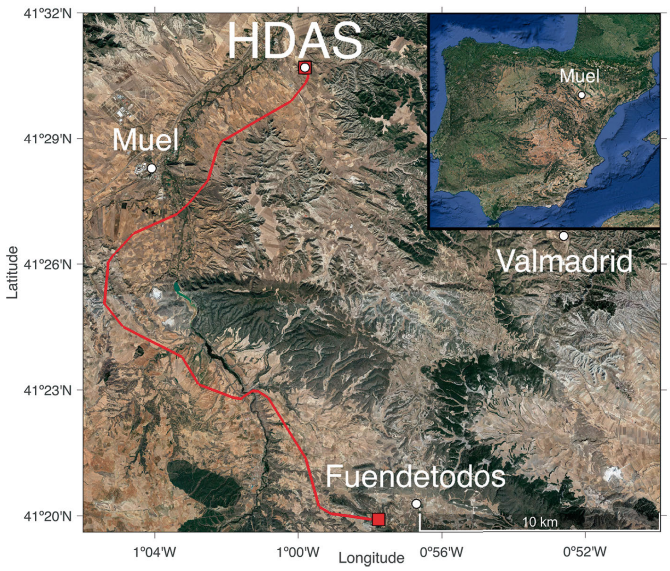

Fig. 1. Location of the experimental installation. The red line indicates the overhead power line installation.

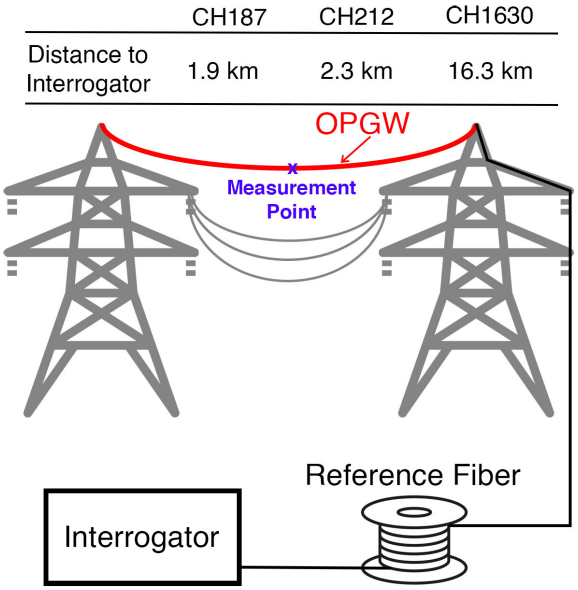

Fig. 2. Experimental measurement installation scheme. Both the interrogator and the reference fiber are located inside a service building in the María substation.

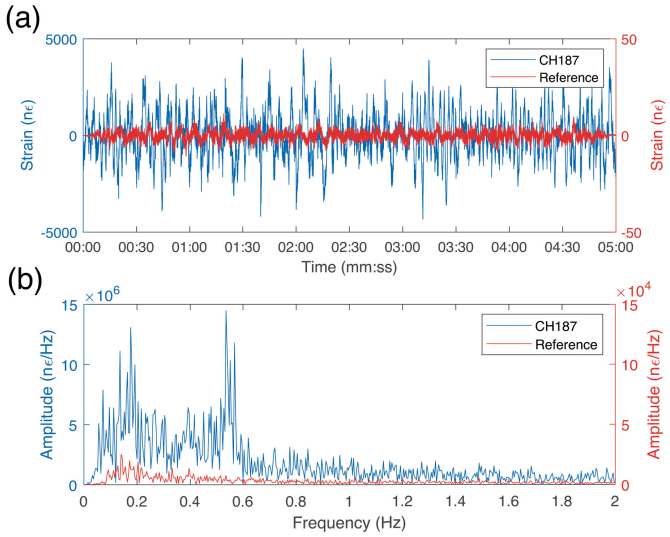

Fig. 3. 5-min data record of CH187 (blue) and launching fiber used as reference (red). (a) Strain. (b) Frequency spectrum.

220-kV lines with optical ground wires (OPGWs) containing several fibers. For this study, one of the dark fibers in the west circuit was used.

The interrogator system was provided and installed by Aragón Photonics Labs in the substation located at the north end of the circuit, in the municipality of María de Huerva. The sampling rate of the interrogator was set to 250 Hz and the channel spacing to 10 m. This interrogator unit, commercially branded as high-fidelity DAS (HDAS), was previously calibrated under the experimental conditions providing a strain resolution up to 1 $n\varepsilon$ and a total sensing distance of 50 km. A launching fiber coil of 1.2-km length was placed between the sensing unit and the connector of the OPGW. This reference fiber was used to compensate for the laser phase noise contribution to the strain measurements. The launching fiber was kept unperturbed by placing it in an isolated foam box inside the substation. By computing the strain recorded in this undisturbed coil, the laser phase noise can be estimated and compensated for the complete monitored fiber, resulting in an improvement of up to 17 dB in the SNR of the measurement [42]. The measurement scheme and the optical fiber length between the measurement points and the interrogator unit are shown in Fig. 2. Measurements were carried out in June 2021.

The strain of a 5-min record (12:00 H, local time) of the central point in the launching fiber, and the channel CH187 are presented in Fig. 3(a). The CH187 is located in the middle point of a 245-m-long span with a northeast transversal direction, around 1.9 km from the interrogator. Previous to any analysis, a 10-s filter is applied to the raw strain data obtained from the interrogator to remove the low-frequency noise derived from high integration times [30]. The spectrum of the strain data for both locations is depicted in Fig. 3(b).

To visualize the different behavior of the points of the fiber, the fast Fourier transform (FFT) of each fiber point has been computed every second and then integrated into the 1–90-Hz range. The integration value is depicted in Fig. 4. It can be clearly seen that there are some areas where the fiber has a higher value for this spectral region than others. The variation of this value along the different locations corresponds to a differential mechanical behavior of the point and is related to a free span of the OPGW between two pylons. By determining the points where there is an abrupt change in this value, all overhead line spans and their respective pylons can be identified. There are also some zones, between spans, where the vibration amplitude decays to really low levels for several meters. These regions correspond to pylons where the fiber within the OPGW goes out of the composite and is coiled in a splicing box due to installation constrictions. The 1.2-km-long fiber span at the beginning of the fiber with a low integrated strain value corresponds to the launching optical fiber coil used for laser noise compensation.

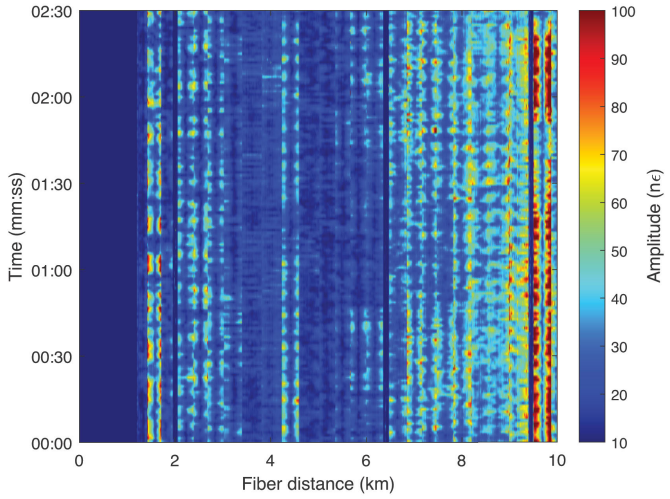

Fig. 4. Optical fiber map with identifiable spans, fiber back-up, and reference fiber.

IV. Sag From Vibration Measurement

The sag of a suspended cable can be directly determined from its vibrational data [16]. Since towers can be assumed to be rigidly fixed, the overhead line can be simplified to a simple cable with no stiffness where both ends are fixed. With this model, each span of the line will present a fundamental frequency that will only depend on the span length and tension in the following equation [43]:

$$f_0 = \frac{1}{2L}\sqrt{\frac{H}{m_c}} \tag{2}$$

where L [m] stands for the conductor's length, H [N] is the conductor's tension, m_c [kg/m] is the mass per unit length of the conductor, and f_0 [Hz] is the fundamental frequency of the vibration mode. The cable structure exhibits both "in-plane" and "out-of-plane" vibration modes, each with multiple harmonic modes, making it challenging to directly observe the fundamental frequency. Equation (3) establishes a direct relationship between the sag of the span taking into account the direct dependence of the sag with the span length, the weight mass of the cable and the tension [15]

$$S = \frac{g}{32}\frac{1}{f_0^2} \tag{3}$$

where S [m] stands for sag and g [m/s^2] is the gravity constant and equal to 9.81 [m/s^2]. Therefore, sag can directly be determined by knowing the fundamental frequency, and it is not influenced by exterior conditions. By monitoring the fundamental frequency, instantaneous sag can be estimated for every span and as it is derived from detected frequencies and not signal amplitude, it does not need any amplitude calibration.

Since the monitoring period occurred during summer, it can be safely assumed that there was no icing on the conductors and thus no changes in mass that could lead to significant contributions to the vibrations. In this scenario, the main variable of the conductor is its length and its temperature. Variations of this parameter are mainly the effect of ambient temperature oscillations and wind exchange, since no Joule effect is present in the OPGW cable [44]. Elongation due to temperature changes also implies tension variations, but both changes are uniquely reflected in the fundamental frequency. As the temperature of the conductor increases and elongation takes place, the sag value is also increased and, following (3), the fundamental frequency of each span inversely decreases. Typical sag values for a 400-m-long span are around 10 m [1], [3], [45], which implies fundamental frequencies around 0.17 Hz [46].

The expected sag of the cable, based on its mechanical characteristics and the distances between pylons, ranges from 5 to 13 m. Elongations due to thermal expansion or contraction can cause the sag to vary below 0.54 m. This corresponds to a fundamental frequency range of 0.25–0.15 Hz, with a variation of 0.01 Hz around the mean value of each span. To achieve the spectral resolution for frequency tracking given these values, a high integration time is required. However, the choice of integration time must balance the required frequency resolution against the duration of perturbations and the occurrence of unexpected high noise events. The integration time should be long enough to achieve sufficient frequency resolution, but not so long that perturbations fade out or that high noise events are captured.

A change in the sag of approximately 0.5 m for the 400-m-long span during the monitored period would correspond to a fundamental frequency variation of 0.01 Hz. To detect oscillations of this mean frequency, a 5-min integration interval was used, which allows for sufficient frequency resolution (1/300 Hz) to detect the expected frequency variations. Although higher integration times result in better frequency resolution, long time spans of acquisition are more likely to be affected by sudden wind gusts which increases the difficulty for the fundamental frequency determination.

By monitoring a fixed fiber point over a long period of time and computing its spectrogram, the fundamental frequency and higher order modes can be observed as featured frequencies with higher strain amplitudes persisting in time. Fig. 5 shows the computed spectrogram of CH187 during a 10-h period with a 300-s integration time. In the frequency range between 0.5 and 2 Hz, the frequency evolution over time is clearly visible and exhibits subtle variations over time. It is worth noting that sudden increases in signal levels occur for wide ranges of points over short periods of time due to wind gusts that overexcite the cable and thus the sensing fiber. This sudden increase is depicted in the spectrogram as vertical stripes. During these periods, the noise level increases, preventing the recovery of any frequency information.

To track the evolution of the frequency value for the different harmonics, depicted in Fig. 5 and correlate them with variations of the sag value, a peak tracking algorithm is applied to the fundamental frequency and the higher-order harmonics, working as Fig. 6 shows. The initial value of the mean frequency is determined using a peak-search algorithm that identifies peaks within a spectrum window based on the expected frequency values for the monitored span. In the next step, the algorithm determines the maximum value of the correlation of the previous peak within a region determined by a

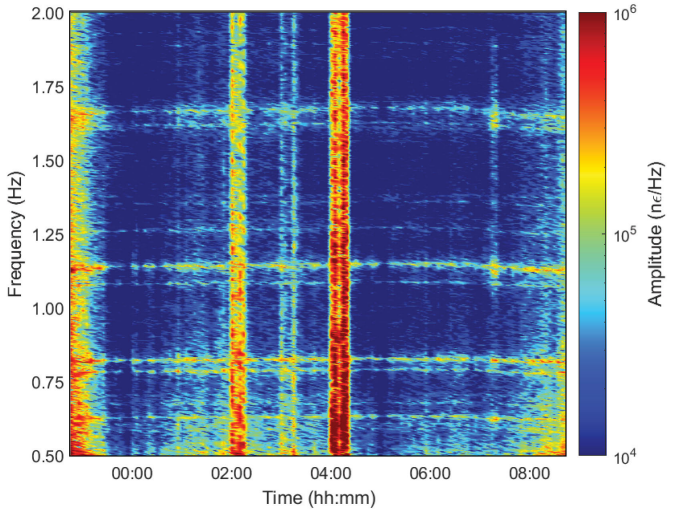

Fig. 5. Spectrogram of CH187 for a 10-h period showing frequency lines and time periods with strong wind.

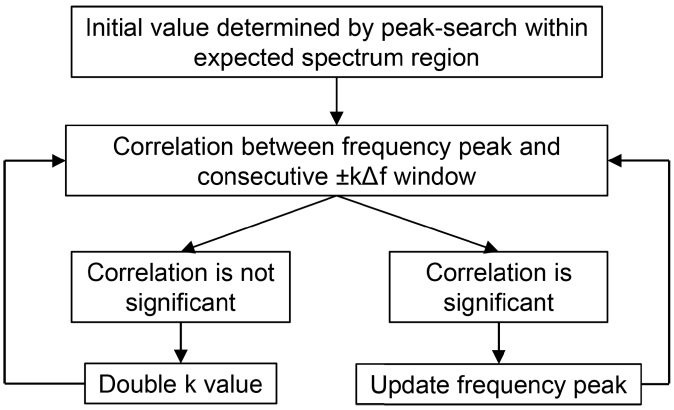

Fig. 6. Frequency line detection algorithm.

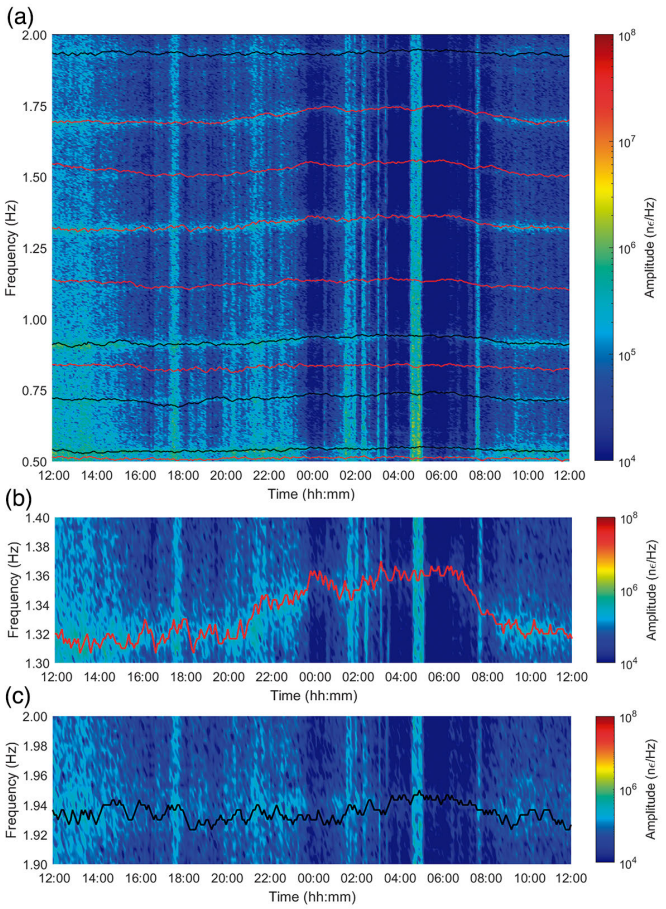

Fig. 7. (a) Frequency lines detected by the algorithm in the 24-h spectrogram of CH1630. Harmonic modes are presented in red, whereas nonharmonic frequencies are displayed in black. (b) Variation of a harmonic mode line during the 24-h period. (c) Evolution of a nonharmonic frequency line.

factor, k, and the frequency resolution of the spectrogram, Δf. If the maximum of the correlation is not significant, the factor k is doubled up to a predefined limit considering the realistic variation within the time span. For the next steps, the factor k is updated according to the position of the previously detected maxima in the correlation so the computational cost is not unnecessarily high.

Although the algorithm exhibits good performance in most of the analyzed lapses of time, when the SNR is low, the maximum of the correlation function may not represent the displacement of the frequency of the oscillations, and a manual discard or selection of the point is needed. A refined algorithm considering the monotonic evolution of the value may avoid these needed manual adjustments, but it was out of the scope of this study. Fig. 7 shows the evolution of the frequency detected for several high-order harmonics by the algorithm in the spectrogram of the signal obtained for the CH1630, which is located in the central point of a 421-m-long span with southwest orientation around 16.3 km far from the measurement device.

The frequencies of the different harmonics show a periodic behavior within a 24-h period. Fig. 8 shows the evolution of the frequency for some of the harmonics together with a polynomial adjustment and the temperature evolution of the 24-h measurement period. It can be noticed that the frequency reaches a maximum value around 05:00 H and a minimum around 18:00 H, corresponding to the time when minimum and maximum environment temperatures have been registered in the meteorological station of Valmadrid, located around 12 km from the power line and owned by the State Meteorological Agency (AEMET). As sag increases linearly with temperature and attending to (3), an inverse relationship between frequency and temperature is expected.

V. Results and Discussion

The frequency variations of the different harmonics have been proved to fluctuate with a comparable periodicity to the temperature changes throughout the day, which is consistent with the anticipated sag variation caused by thermal expansion or contraction [47]. However, (3) allows for a quantitative determination of the sag, provided the fundamental mode is calculated. Fig. 7 shows the evolution of multiple frequencies over time. The fundamental frequency can be obtained by finding the greatest common divisor of all of them at a certain time. However, not all lines in Fig. 7 can be obtained as multiples of the same fundamental value. In this case,

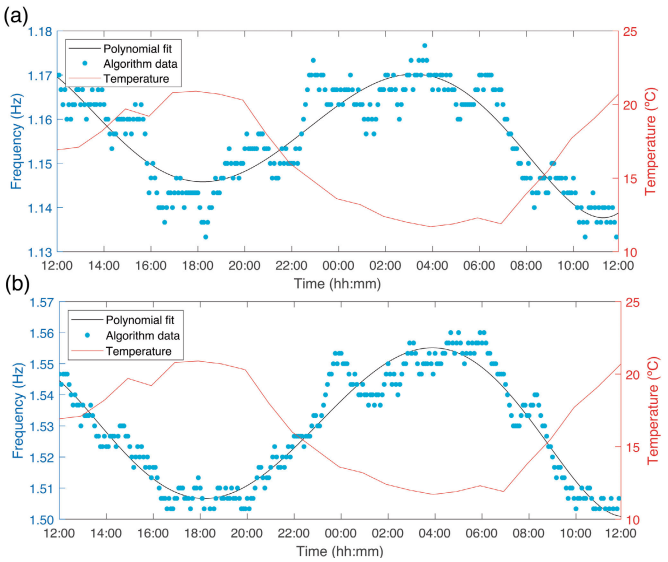

Fig. 8. Evolution of frequency lines compared with temperature for CH1630. (a) 1.16-Hz line (seventh harmonic). (b) 1.51-Hz line (ninth harmonic).

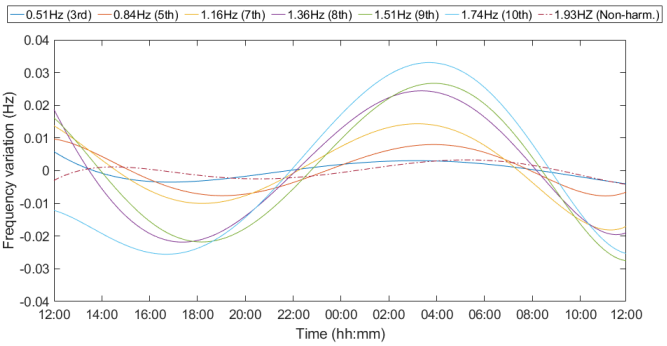

Fig. 9. Frequency evolution of harmonic modes for CH1630 during the 24-h measurement period.

there are several values that cannot be correlated to the same fundamental frequency. Nevertheless, these values do not exhibit any evolution over the course of the day and they are likely to be correlated with mechanical oscillations of the tower that are transferred to the cable [48] or other vibration phenomena [49]. Fig. 9 shows the evolution of the frequency of six harmonics throughout the day, as well as the static value for one frequency that is not related to the same fundamental frequency as the other harmonics. It can be observed that the higher the order of the harmonic, the greater the excursion of the central frequency. The fundamental frequency corresponding to these harmonics is 0.169 Hz, and thus the harmonics represented are the third, fifth, seventh, eighth, ninth, and tenth. By using the fundamental frequency from all the before-mentioned modes and (3), the absolute sag values can be monitored for the 24-h measured period. Fig. 10 shows the evolution of the sag value for CH1630 and the temperature evolution for the monitored lapse of time.

To validate the quantified value of the sag, on-field measurement was performed by using a laser telemeter to measure the distance from the lowest point of the OPGW to the ground. Due to limited terrain accessibility, the position for the on-site

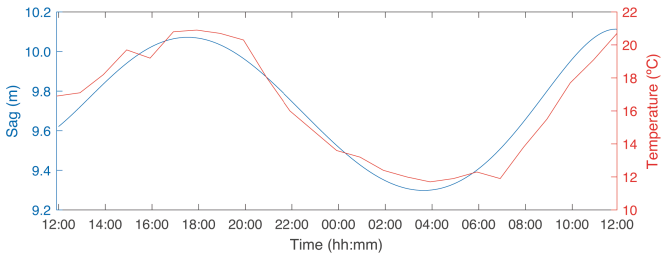

Fig. 10. Sag evolution in the 24-h period for CH1630 obtained using the HDAS.

TABLE I
SAG DIFFERENCE FOR TELEMETER AND HDAS MEASUREMENTS

	Distance to ground (Telemeter) [m]	**Sag values** (HDAS) [m]
Measurement at 7:30H	34.65	7.23
Measurement at 15:00H	33.96	7.84
Difference	0.69	0.61

analysis corresponds to the CH212 that lies in the middle point of a 343.51 m span and is 2258 m away from the interrogator unit. This measurement was taken at two different times during the same day for the same point when the temperature difference was significant. The difference between these two on-site measurements corresponds to the amplitude evolution of the sag for that point. At the same time, the sag difference was estimated using the HDAS for the same point. Both values are displayed in Table I. It is observed that the values obtained with the HDAS frequency monitoring method are in great accordance with the on-site measured values. Although these values prove that the described method results in a useful solution for the sag measurement challenge, there are external factors that can reduce the accuracy of the described technique. The most relevant of these factors is the presence of sudden and strong wind gusts. This phenomenon reduces the ability to identify the featured frequencies in the temporal windows where it takes place. However, a temporal analysis of the strain could allow for dynamically adapting the integration window and discarding those instances that present high noise levels. This adaptive approach, although it would come with a higher computational cost, would increase the robustness of the method and thus improve its overall accuracy.

VI. CONCLUSION

In this work, a 31.8-km-long overhead line was monitored using a CP-ΦOTDR to study the vibration-induced strain on the fiber. The spectrograms of the registered strain along the fiber were obtained, and multiple local maxima at different frequencies were observed. These peaks account for all the vibration phenomena that are happening in the cable. Some of these frequency peaks exhibit a 24-h periodic variation that can be correlated with the ambient temperature changes. These peaks are correlated to the sag for each span and the frequency excursion of the peaks is directly related to the elongation and contraction of the cable due to thermal dilation. A careful identification of the harmonics and a thorough analysis of these frequencies enable the determination of the fundamental

frequency. This value enables the quantitative calculation of the sag value. By tracking this fundamental frequency throughout the day, the sag has been monitored across the overhead line. To validate the results, on-site measurements were taken, showing great accordance with the results estimated with the fundamental frequency estimation through the strain analysis. This method allows for a distributed measurement, overcoming the main drawbacks of the current point-wise sag monitoring techniques.

ACKNOWLEDGMENT

The authors would like to thank the State Meteorological Agency (AEMET) for providing the climatological information.

REFERENCES

[1] A. H. Khawaja, Q. Huang, J. Li, and Z. Zhang, "Estimation of current and sag in overhead power transmission lines with optimized magnetic field sensor array placement," *IEEE Trans. Magn.*, vol. 53, no. 5, pp. 1–10, May 2017.

[2] Z.-W. Ding et al., "Phi-OTDR based on-line monitoring of overhead power transmission line," *J. Lightw. Technol.*, vol. 39, no. 15, pp. 5163–5169, Aug. 2021.

[3] D. A. Douglass and F. R. Thrash, *Sag and Tension of Conductor*. Boca Raton, FL, USA: CRC Press, Sep. 2018.

[4] F. I. Oluwajobi, O. S. Ale, and A. Ariyanninuola, "Effect of sag on transmission line," *J. Emerg. Trends Eng. Appl. Sci.*, vol. 3, no. 4, pp. 627–630, Aug. 2012.

[5] Y. Zhang, X. Yuan, W. Li, and S. Chen, "Automatic power line inspection using UAV images," *Remote Sens.*, vol. 9, no. 8, p. 824, Aug. 2017.

[6] P. Patowary and N. Goyal, "Overload security and risk assessment of overhead lines," in *Proc. 6th IEEE Power India Int. Conf. (PIICON)*, Dec. 2014, pp. 1–6.

[7] A. Michiorri et al., "Forecasting for dynamic line rating," *Renew. Sustain. Energy Rev.*, vol. 52, pp. 1713–1730, Dec. 2015.

[8] T. S. Hlalele and S. Du, "Real time monitoring of high voltage transmission line conductor sag: The state-of-art," *Int. J. Eng. Adv. Technol.*, vol. 3, no. 1, pp. 297–302, Oct. 2013.

[9] X. Dong, "Analytic method to calculate and characterize the sag and tension of overhead lines," *IEEE Trans. Power Del.*, vol. 31, no. 5, pp. 2064–2071, Oct. 2016.

[10] S. Kamboj and R. Dahiya, "Case study to estimate the sag in overhead conductors using GPS to observe the effect of span length," in *Proc. IEEE PES T&D Conf. Expo.*, Apr. 2014, pp. 1–4.

[11] A. Molaei, H. D. Taghirad, and J. Dargahi, "Extracting of sagging profile of overhead power transmission line via image processing," in *Proc. IEEE Can. Conf. Electr. Comput. Eng. (CCECE)*, May 2018, pp. 1–5.

[12] E. Golinelli, U. Perini, and G. Ogliari, "A new IR laser scanning system for power lines SAG measurements," in *Proc. 18th Italian Nat. Conf. Photonic Technol. (Fotonica)*, Jun. 2016, pp. 1–4.

[13] A. T. Zengin, G. Erdemir, T. C. Akinci, and S. Seker, "Measurement of power line sagging using sensor data of a power line inspection robot," *IEEE Access*, vol. 8, pp. 99198–99204, 2020.

[14] R. Miller, F. Abbasi, and J. Mohammadpour, "Power line robotic device for overhead line inspection and maintenance," *Ind. Robot, Int. J.*, vol. 44, no. 1, pp. 75–84, Jan. 2017.

[15] B. Godard, "A vibration-sag-tension-based icing monitoring of overhead lines," in *Proc. Int. Workshop Atmos. Icing Struct.*, Jun. 2019, pp. 1–7.

[16] E. Cloet and J-L. Lilien, "Uprating transmission lines through the use of an innovative real-time monitoring system," in *Proc. IEEE PES 12th Int. Conf. Transmiss. Distrib. Construct., Operation Live-Line Maintenance (ESMO)*, May 2011, pp. 1–6.

[17] D. Dumitru, "Modelling the growth of wind-induced oscillations in overhead lines. Non-resonant case," *Ann. Constanţa Maritime Univ.*, vol. 16, no. 24, pp. 207–212, Jul. 2015.

[18] L. Zhao, X. Huang, Y. Zhang, Y. Zhu, J. Jia, and C. Zhu, "Aeolian vibration-based structural health monitoring system for transmission line conductors," *Struct. Control Health Monitor.*, vol. 27, no. 6, p. 2538, Jun. 2020.

[19] L. Zhao, X. Huang, J. Jia, Y. Zhu, and W. Cao, "Detection of broken strands of transmission line conductors using fiber Bragg grating sensors," *Sensors*, vol. 18, no. 7, p. 2397, Jul. 2018.

[20] G. Fusiek and P. Niewczas, "Design of an optical sensor with varied sensitivities for overhead line sag, temperature and vibration monitoring," in *Proc. IEEE Int. Instrum. Meas. Technol. Conf. (I2MTC)*, May 2022, pp. 1–6.

[21] A. U. Mahin, S. N. Islam, F. Ahmed, and M. F. Hossain, "Measurement and monitoring of overhead transmission line sag in smart grid: A review," *IET Gener., Transmiss. Distrib.*, vol. 16, no. 1, pp. 1–18, Jan. 2022.

[22] M. Wydra, P. Kisala, D. Harasim, and P. Kacejko, "Overhead transmission line sag estimation using a simple optomechanical system with chirped fiber Bragg gratings. Part 1: Preliminary measurements," *Sensors*, vol. 18, no. 1, p. 309, Jan. 2018.

[23] K. Skorupski et al., "Overhead transmission line sag estimation using the simple opto-mechanical system with fiber Bragg gratings—Part 2: Interrogation system," *Sensors*, vol. 20, no. 9, p. 2652, May 2020.

[24] H. Singh, G. Fusiek, and P. Niewczas, "Extended characterization of an optical sag sensor for high-temperature low-sag lines," *IEEE Sensors Lett.*, vol. 7, no. 9, pp. 1–4, Sep. 2023.

[25] G. Fusiek, H. Singh, and P. Niewczas, "Temperature and force characterization of an optical sag sensor for overhead line monitoring," in *Proc. IEEE Int. Instrum. Meas. Technol. Conf. (I2MTC)*, May 2023, pp. 1–5.

[26] G.-m. Ma et al., "Ice monitoring on overhead transmission lines with FBG tension sensor," in *Proc. Asia–Pacific Power Energy Eng. Conf.*, Mar. 2010, pp. 1–4.

[27] N. Q. Mao, G. M. Ma, H. Y. Zhou, C. R. Li, and Y. B. Li, "The online monitoring system of transmission lines weight based on fiber sensing technology," in *Proc. Int. Conf. Condition Monitor. Diagnosis (CMD)*, Sep. 2016, pp. 635–638.

[28] P. Munster et al., "Φ-OTDR signal amplification," *Opt. Sensors*, vol. 9506, pp. 28–36, May 2015.

[29] B. Godard, S. Guerard, and J.-L. Lilien, "Original real-time observations of aeolian vibrations on power-line conductors," *IEEE Trans. Power Del.*, vol. 26, no. 4, pp. 2111–2117, Oct. 2011.

[30] Y. Muanenda, C. J. Oton, and F. Di Pasquale, "Application of Raman and Brillouin scattering phenomena in distributed optical fiber sensing," *Frontiers Phys.*, vol. 7, p. 155, Oct. 2019.

[31] L. Palmieri, "Distributed optical fiber sensing based on Rayleigh scattering," *Open Opt. J.*, vol. 7, no. 1, pp. 104–127, 2013.

[32] E.-G. Neumann, *Single-Mode Fibers: Fundamentals*, vol. 57. Cham, Switzerland: Springer, 2013.

[33] Z. Wang, H. Wu, X. Hu, N. Zhao, Q. Mo, and G. Li, "Rayleigh scattering in few-mode optical fibers," *Sci. Rep.*, vol. 6, no. 1, Oct. 2016, Art. no. 35844.

[34] S. Girard et al., "Overview of radiation induced point defects in silica-based optical fibers," *Rev. Phys.*, vol. 4, Nov. 2019, Art. no. 100032.

[35] M. Imahama, Y. Koyamada, and K. Hogari, "Restorability of Rayleigh backscatter traces measured by coherent OTDR with precisely frequency-controlled light source," *IEICE Trans. Commun.*, vol. E91-B, no. 4, pp. 1243–1246, Apr. 2008.

[36] F. Peng, H. Wu, X.-H. Jia, Y.-J. Rao, Z.-N. Wang, and Z.-P. Peng, "Ultra-long high-sensitivity Φ-OTDR for high spatial resolution intrusion detection of pipelines," *Opt. Exp.*, vol. 22, no. 11, pp. 13804–13810, 2014.

[37] H. Gabai and A. Eyal, "On the sensitivity of distributed acoustic sensing," *Opt. Lett.*, vol. 41, no. 24, p. 5648, Dec. 2016.

[38] Z. Wang et al., "Coherent Φ-OTDR based on I/Q demodulation and homodyne detection," *Opt. Exp.*, vol. 24, no. 2, pp. 853–858, Jan. 2016.

[39] J. Pastor-Graells, H. F. Martins, A. Garcia-Ruiz, S. Martin-Lopez, and M. Gonzalez-Herraez, "Single-shot distributed temperature and strain tracking using direct detection phase-sensitive OTDR with chirped pulses," *Opt. Exp.*, vol. 24, no. 12, p. 13121, Jun. 2016.

[40] Y. Koyamada, M. Imahama, K. Kubota, and K. Hogari, "Fiber-optic distributed strain and temperature sensing with very high measurand resolution over long range using coherent OTDR," *J. Lightw. Technol.*, vol. 27, no. 9, pp. 1142–1146, May 2009.

[41] M. R. Fernández-Ruiz, L. Costa, and H. F. Martins, "Distributed acoustic sensing using chirped-pulse phase-sensitive OTDR technology," *Sensors*, vol. 19, no. 20, p. 4368, Oct. 2019.

[42] M. R. Fernández-Ruiz, J. Pastor-Graells, H. F. Martins, A. Garcia-Ruiz, S. Martin-Lopez, and M. Gonzalez-Herraez, "Laser phase-noise cancellation in chirped-pulse distributed acoustic sensors," *J. Lightw. Technol.*, vol. 36, no. 4, pp. 979–985, Feb. 2018.

[43] H. M. Irvine, *Cable Structures*. New York, NY, USA: Dover, 1992.
[44] J. Fu, S. Abbott, B. Fox, D. J. Morrow, and S. Abdelkader, "Wind cooling effect on dynamic overhead line ratings," in *Proc. 45th Int. Universities Power Eng. Conf. UPEC*, Aug. 2010, pp. 1–6.
[45] R. G. Olsen and K. S. Edwards, "A new method for real-time monitoring of high-voltage transmission-line conductor sag," *IEEE Trans. Power Del.*, vol. 17, no. 4, pp. 1142–1152, Oct. 2002.
[46] X. Liu, Y. Hu, and M. Cai, "Free vibration analysis of transmission lines based on the dynamic stiffness method," *Roy. Soc. Open Sci.*, vol. 6, no. 3, Mar. 2019, Art. no. 181354.
[47] I. Albizu, A. J. Mazón, V. Valverde, and G. Buigues, "Aspects to take into account in the application of mechanical calculation to high-temperature low-sag conductors," *IET Gener., Transmiss. Distrib.*, vol. 4, no. 5, p. 631, 2010.
[48] H. Maeda, S. Ebihara, M. Fujimura, J. Maeda, Y. Imamura, and M. Honda, "Vibration tests of a tranmission tower focusing on the tensile forces of its transmission line cables," in *Proc. 16th Conf. Electr. Power Supply Ind.*, 2006, pp. 1579–1588.
[49] C. Hickey, P. Young, T. Mayomi, and J. Noctor, "Fault investigation and analysis of an overhead transmission line vibration damper," in *Proc. 56th Int. Universities Power Eng. Conf. (UPEC)*, Aug. 2021, pp. 1–6.

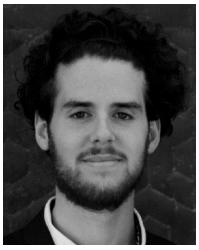

Jorge Canudo was born in Zaragoza, Spain. He received the bachelor's degree in physics and the master's degree in physics and physical technologies from the Universidad de Zaragoza, Zaragoza, Spain, in 2022 and 2023, respectively, where he is currently pursuing the Ph.D. degree with the Photonics Technologies Group (GTF).

His research interests are focused on high-resolution distributed acoustic sensors (DASs) and their applications.

Pascual Sevillano was born in Santa Cruz de Tenerife, Spain. He received the M.Sc. and Ph.D. degrees in physics from the Universidad de Zaragoza, Zaragoza, Spain, in 2010 and 2015, respectively.

From 2015 to 2020, he worked at Aragon Photonics Labs, Zaragoza, where he was the Head of the Research and Development Department. In 2020, he joined the Department of Applied Physics, Universidad de Zaragoza, as an Assistant Professor. In 2021, he became a member of the Engineering Research Institute of Aragon (I3A), Zaragoza. His research interests are mainly focused on nonlinear optical phenomena in fiber and its application in distributed sensing.

Andrea Iranzo was born in Zaragoza, Spain. She received the bachelor's degree in physics from the Universidad de Zaragoza, Zaragoza, in 2020, and the master's degree in advanced physics and photonics from the University of Valencia, Valencia, Spain, in 2021.

Since 2022, she has been working at Aragon Photonics Labs, Zaragoza, as a Research and Development Engineer.

Sacha Kwik was born in Palma (Mallorca), Spain. He received the bachelor's degree in telecommunications engineering from the University of the Balearic Islands, Palma, in 2006, the M.Sc. degree in telecommunications engineering and management from UPC-Barcelona Tech University, Barcelona, Spain, in 2008, and the M.Sc. degree in projects, deployment, and maintenance of electric high-voltage infrastructures from Comillas University, Madrid, Spain, in 2015.

Since 2010, he has been working at the Spanish Electrical Transmission and System Operator, Red Eléctrica, Alcobendas, Spain, where he specialized in fiber-optic networks and monitoring systems.

Javier Preciado-Garbayo was born in Pamplona, Spain, in 1990. He received the bachelor's degree in telecommunications technology and services engineering and the master's degree in telecommunications engineering from the Universidad de Zaragoza, Zaragoza, Spain, in 2015 and 2017, respectively.

During the second year of the master's degree, he was part of the Erasmus Exchange Program in Linköping University, Linköping, Sweden. In 2023, he finished his industrial Ph.D. focused on Distributed Optical Fiber Sensors (DOFs) "Integración de sistemas de sensado distribuido sobre fibra óptica y estudio de aplicaciones de uso" at Aragon Photonics Labs, Zaragoza, where he is Technical Leader in the Sensing Division.

Jesús Subías received the M.Sc. and Ph.D. degrees in physics from the Universidad de Zaragoza, Zaragoza, Spain, in 1991 and 1996, respectively.

In 1991, he joined the Department of Applied Physics, Universidad de Zaragoza, where he was an Assistant Professor, from 1994 to 1999, and he has been an Associate Professor, since 2000. His current research interests include optical fiber systems, test and measurement, and nonlinear effects in optical fibers.